Journal of Materials Science: Materials in Electronics (2018) 29:13292–13301
https://doi.org/10.1007/s10854-018-9453-x

Highly efficient light responsive BiOCl/AgI composites for photocatalytic degradation of 3-CP under visible and UV light irradiations

Ali İmran Vaizoğullar[1]

Received: 3 January 2018 / Accepted: 8 June 2018 / Published online: 12 June 2018

Abstract
Novel visible light sensitive BiOCl/AgI composites were synthesized by a facile precipitation technique. Samples were characterized by SEM (scanning electron microscope), XRD (X-ray diffraction), UV-DRS (UV-diffuse reflectance spectroscopy) and XPS (X-ray photoelectron spectroscopy). Photocatalytic activity of the samples was evaluated using 3-CP under UV–Visible irradiation. Compared to pure BiOCl, AgI and other BiOCl/AgI, the composites exhibited more catalytic activity under both UV and visible lights within 120 min. Optimal content of the BiOCl in the composite system was found as 40%. The excellent degradation of 3-CP under light was attributed to the efficient separation of photo-induced charge carriers, defect levels, iodide and chlorine ($I^{\cdot}$, $Cl^{\cdot}$) radicals. The radical scavenging activities also illustrate that holes and superoxide radicals (h^{+}) and ($O_2^{-\cdot}$) are dominant agents in the photocatalytic degradation process. These results demonstrated that BiOCl/AgI systems are very useful to decompose persistent organic pollutants.

1 Introduction

Water pollution, especially having organic contamination and harmful bacteria, is a serious growing problem due to industrialization as well as economic and population growth [1]. Dealing organic pollutants has become an urgent concern [2]. Toxic metabolites exhibit harmful effects on human beings and other living organisms [3]. As an example, chlorinated phenols that exist in the ecosystem are very toxic to almost all organisms. Aromatic chlorinated phenols cause death or reflects serious side effects; even at very low concentrations [4].

To treat organic pollutants in water, different methods have been applied such as biodegradation, adsorption, direct UV light [5], flocculation, electrochemical treatment etc [6, 7]. However, these techniques have certain disadvantages such as high energy consumption, low removing yields, production of toxic intermediates etc. Therefore, the fabrication of efficient and eco-friendly materials has become compulsory.

There has been an increasing interest in advanced oxidation process (AOPs) where organic pollutants are mineralized by generating radicals such as hydroxyl ($OH^{-\cdot}$) or superoxide ($O_2^{-\cdot}$) [8]. The reported photocatalytic systems are based on TiO_2, ZnO, ZnS, AgBr and AgCl [9]. Recent developments in the Bi-based photocatalyst have led to a renewed interest in the catalytic procedures. Especially, Bi-based oxyhalides have been studied due to their unique properties [10].

BiOCl is an important Bi-based material to study in the photocatalytic reactions. It has anisotropic material with $[Bi_2O_2]^{2+}$ layers by intercalated Cl^{-} ions. This presents an internal electric field in the BiOCl structure that results in the effective separation of electron–hole pairs, which provides enhanced catalytic performance under light [11]. In addition, Ag-based photo-catalysts are used as well to enhance catalytic performance [12]. AgX reveals an electron and hole pairs by absorbing photon under visible light. Ag and Bi-based catalysts such as AgI/Ag_2CO_3, and $BiOCl/TiO_2$ have been showed higher catalytic activity than their pure forms. The results reflected by these materials has suggested that heterojunction materials could help in the inhibition of photogenerated species and further enhance the light response and photocatalytic performance of Ag or Bi-based hybrids.

✉ Ali İmran Vaizoğullar
aliimran@mu.edu.tr

[1] Vocational School Health Care, Medical Laboratory Programme, Muğla Sıtkı Koçman University, Muğla, Turkey

To the best of our knowledge, there is no report where BiOCl/AgI composites are used in the photocatalytic degradation of 3-CP. Herein we report the preparation of BiOCl/AgI composites by an in situ precipitation method. Composites were subjected to the photocatalytic degradation against 3-CP under UV–Visible irradiation. The morphology, optical properties and structure of the composites were also evaluated. The purpose of this investigation was to relate AgI and BiOCl.

2 Experimental

2.1 Synthesis of AgI

25 mL of silver nitrate ($AgNO_3$ 0.1 mol L^{-1}) and 20 mL of potassium iodide (KI 0.15 mol L^{-1}) were stirred in a beaker for 60 min at room temperature in dark. The obtained yellowish-green particles were filtered, washed with distilled water/ethanol mixture (80v/20v) and dried at 90 °C for 180 min.

2.2 Synthesis of BiOCl-bent

A solution of 5.28 g of $Bi(NO_3)_3{\cdot}5H_2O$ in 25 mL of concentrated HCl was stirred for 4 h at room temperature. The mixture was aged for 12 h. The obtained solid particles were dried at 85 °C for 3 h and calcined at 200 °C for 4 h.

2.3 Preparation of BiOCl/AgI composites

The BiOCl/AgI composites were obtained by in situ precipitation technique. For this purpose, an appropriate amount of BiOCl was added to 50 mL of distilled water. Then, 1 gr of silver nitrate and 35 mL of potassium iodide (0.1 M) were added and stirred in the dark for 120 min. The obtained product was filtered, washed with distilled water/ethanol (80v/20v) and dried at 90 °C for 120 min. A series of BiOCl/AgI composites were prepared with different weight ratios of BiOCl. 25, 40, 50% BiOCl particles were defined as 25BAg, 40BAg and 50BAg respectively.

2.4 Characterization

Microstructure and shape of the particles were investigated using SEM (JEOL JSM-7600F). Transmission electron micrographs (TEM) were obtained from JEOL JEM-2100 (UHT) microscope. Crystalline structure was examined by XRD (Rigaku Dmax 350) using copper K radiation ($\lambda = 0.154056$ nm). The photoluminescence (PL) emission spectra of the samples were recorded by a spectrofluorometric (Spex 500 M, USA). Optical properties were performed using UV–Vis 1601 spectrophotometer (Dr. Lange 1601 UV–Vis spectrophotometer) at room temperature. X-Ray photoelectron spectroscopies (XPS) measurement was performed using PHI 5000 Versa Probe.

3 Result and discussion

3.1 XRD analysis

The XRD result of AgI and BiOCl/AgI samples are provided in Fig. 1. All diffraction peaks are sharp that indicates well crystallite structure of the prepared samples. Characteristic diffraction peaks of BiOCl were observed at $2\theta = 11.98°$, 25.86°, 32.45°, 33.45°, 40.95°, 46.33°, 49.66°. These values correspond to the tetragonal structure of BiOCl with (001), (002), (110), (012), (112), (020), and (113) planes, respectively (Fig. 1a) [13].

Moreover, pure AgI shows sharp diffraction peaks at $2\theta = 22.31°$, 23.70°, 25.37°, 32.80°, 39.09°, 42.62° and 46.23° (Fig. 1) that corresponds to the (100), (002), (101), (102), (110), (103), (112) crystal planes of β-phase AgI crystal [14]. The peak intensity ratio of (110) to (001) planes for BiOCl was calculated as 2.32, 2.26 and 2.53 for 25BAg, 40BAg and 50BAg samples, respectively. It is possible that AgI particles were more dispersed onto (001) facet in the 40BAg sample (Fig. 1b).

It is clear that addition of BiOCl did not change the diffraction peaks of AgI in the AgI–BiOCl samples as compared with the standard AgI in the JPDS pattern. For the AgI–BiOCl samples, the intensity of diffraction peaks of BiOCl are gradually increased (Fig. 1b). The XRD patterns of the synthesized catalysts were evaluated with the standard card of Ag (JCPDS No. 04-0783). Metallic Ag (green line in Fig. 1b) was not obtained the prepared samples [15]. After producing BiOCl/AgI, the peaks of the composites remarkably shifted to higher 2 theta angle with the increasing of BiOCl content, which confirms a strong interaction between AgI and BiOCl (Fig. 1c).

3.2 SEM analysis

All composites showed almost similar morphology that confirms the co-existing of BiOCl and AgI (Fig. 2). Two types of shapes were observed in the composites samples. AgI particles were collected on the surface of BiOCl. The surfaces of the composite samples were rough that presented higher sorption onto their surfaces, that is why efficient catalytic degradation occured. As shown in Fig. 2d, BiOCl particles have platelet morphology of 50–70 nm thickness with semi-uniform flat surfaces.

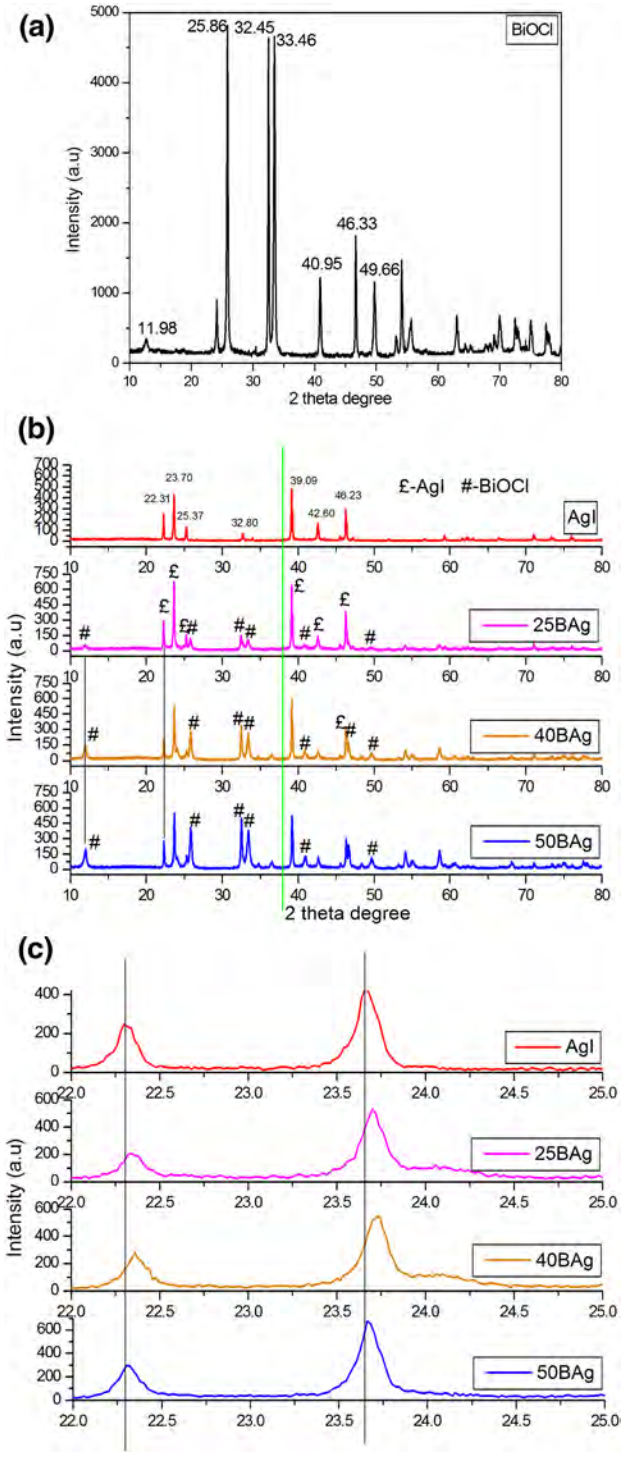

Fig. 1 XRD pattern of pure BiOCl (**a**), all samples (**b**) and shifting of 2θ degree (**c**)

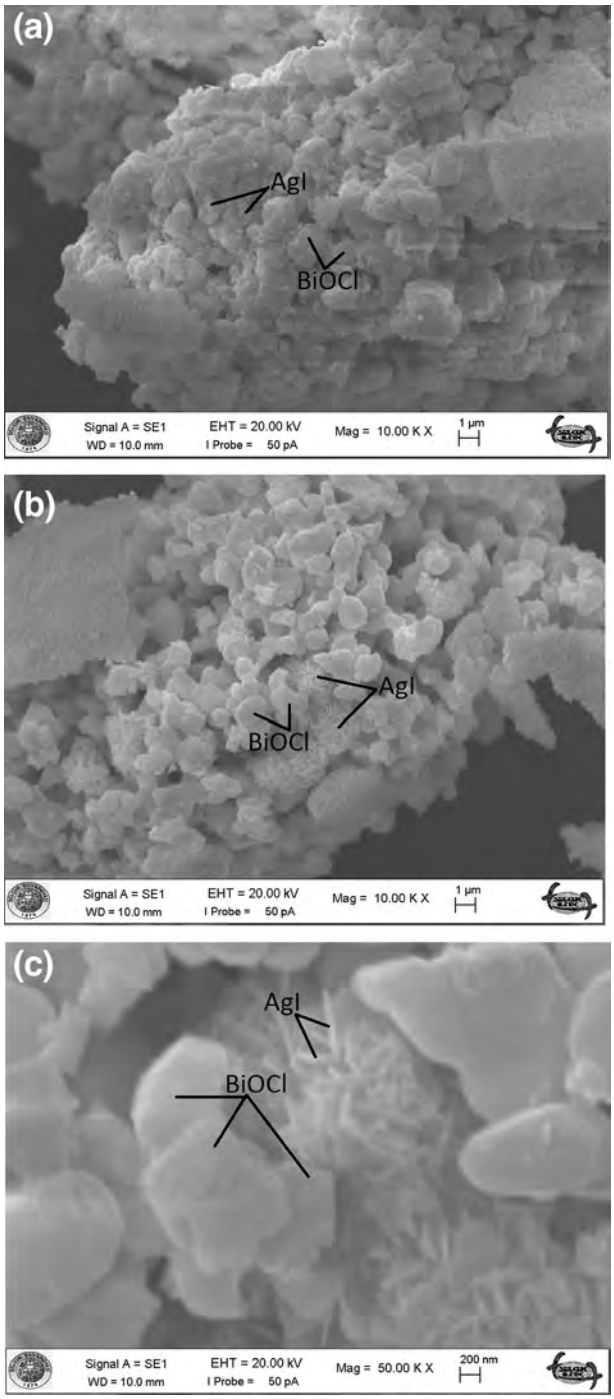

Fig. 2 SEM images of the synthesized composite particles 25BAg (**a**), 40BAg (**b**), 50BAg (**c**)

3.3 TEM analysis

Figure 3 shows TEM image AgI/BiOCl (40BAg) composite. From Fig. 3a, it can be seen that the AgI and BiOCl were combined closely (Fig. 3a). BiOCl and AgI particles were spherical and rods shapes. The EDX mapping images exhibits that AgI/BiOCl (40BAg) sample shows a uniform distribution of the chemical elements on their surfaces. Hence, it could conceivably be hypothesized that BiOCl and AgI co-exist in the composite photocatalyst with close interaction.

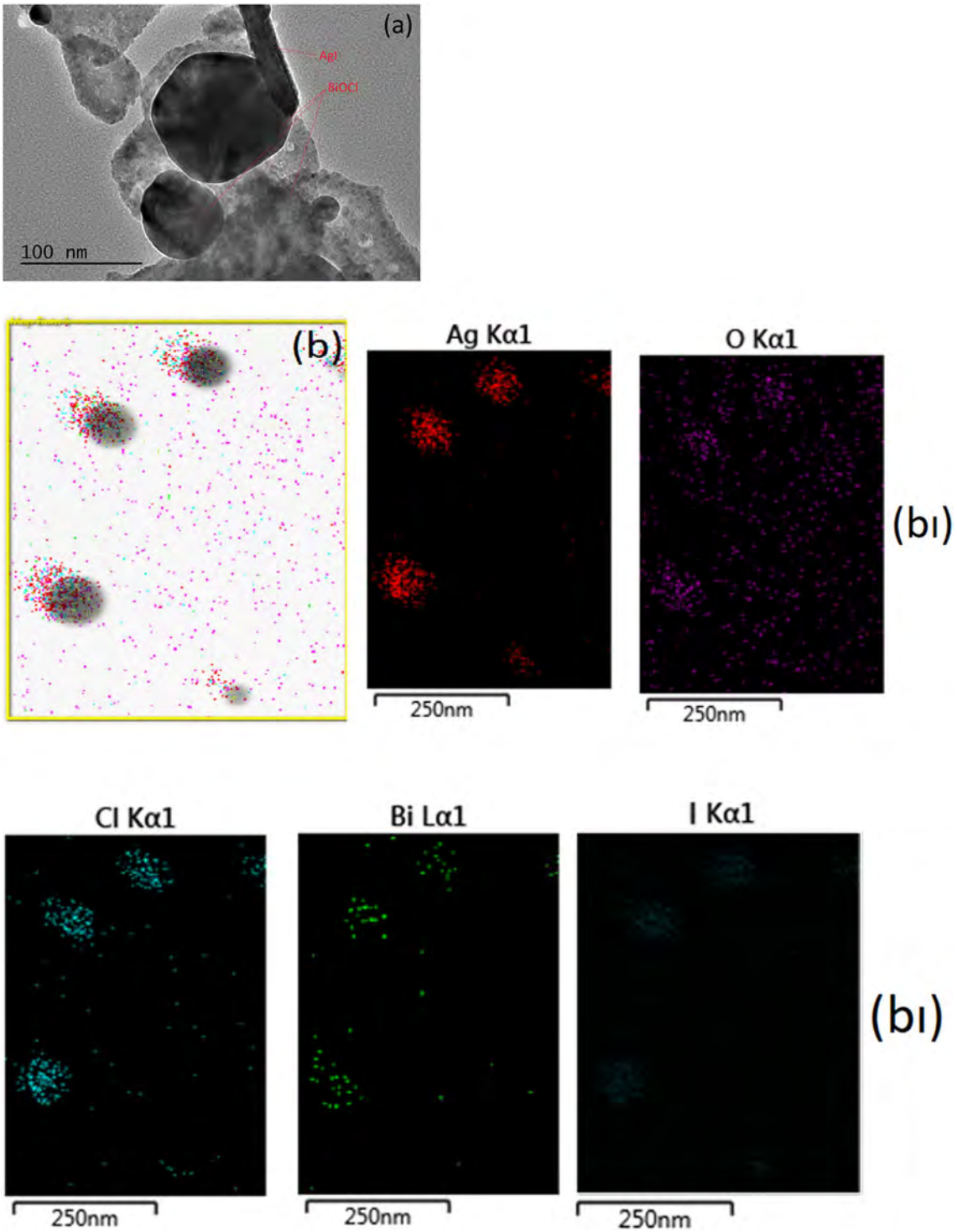

Fig. 3 TEM image (**a**) and corresponding elemental mapping images (**b, bı**) of 40BAg nanoparticles

3.4 Optical properties

The optical properties of catalysts play a major role in the photosensitization activity. UV–Vis analysis was performed between 200 and 800 nm spectral ranges to investigate the optical and light-acting properties of the samples. Figure 4a presents the UV–Vis diffuse reflectance spectra of BiOCl, AgI and BiOCl/AgI. All samples (except BiOCl) absorbed the visible light of <450 nm suggesting their broad utility under the visible light irradiation. Band gap values (Table 1)

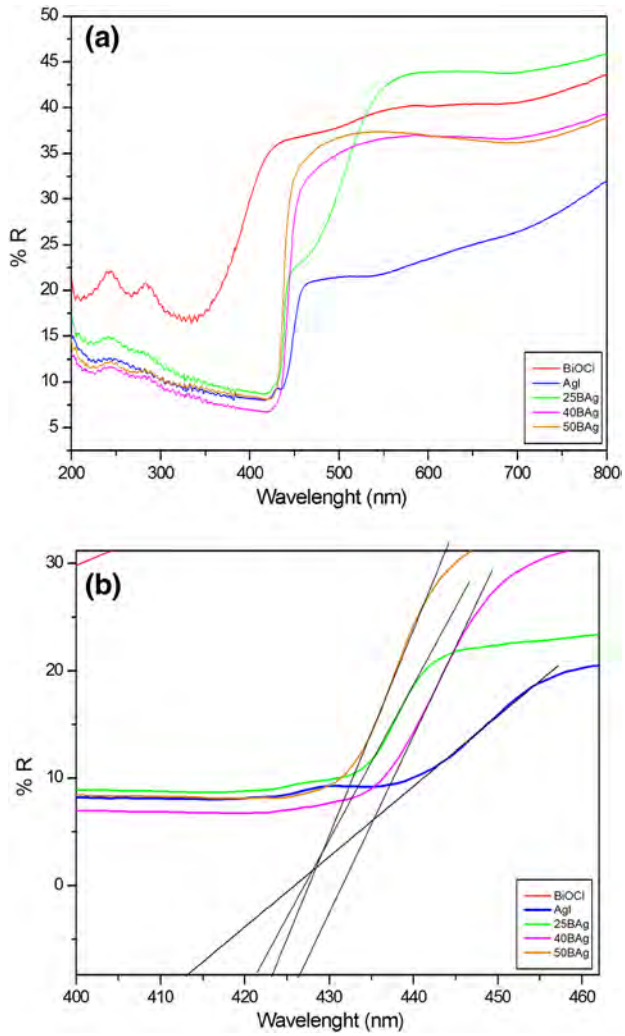

Fig. 4 UV-DRS spectra of the synthesized samples

Table 1 Band gaps and kinetic results of the catalysts

Photocatalyst	Band gap (eV)	Visible light		UV light	
		k (min^{-1}) (10^{-3})	R^2	k (min^{-1}) (10^{-3})	R^2
Blank	–	0.1	0.68	0.1	0.68
BiOCl	4.31	2.2	0.99	3.2	0.95
AgI	3.01	3.4	0.99	4.3	0.99
25Bag	2.93	4.2	0.99	6.1	0.98
40Bag	2.91	6.5	0.98	10.7	0.98
50BAg	2.92	4.6	0.98	8.8	0.99

of the samples were calculated using $E_g = \frac{1240}{\lambda}$ formula. The band gap value of BiOCl is higher than the others.

As well known, crystalline structure and surface properties can change the DRS results of a catalyst. With the increasing of BiOCl content, slightly red shift occurs that can be seen in the spectrum of BiOCl/AgI composites that is in fact caused by the synergetic effect between BiOCl and AgI [16]. However, no noticeable differences were observed in the band gap values of the synthesized BiOCl/AgI catalysts. The band gap value of the 40BAg sample is lower as compared to the values of other composites (Table 1). A possible explanation for this case can be oxygen vacancy that provides a new electronic state in the BiOCl, which acts as a trap to capture excited electrons. This phenomenon is useful to expand the absorption spectrum to the visible light region [17].

In summary, the obtained band gap values of the BiOCl and AgI are smaller than that of BiOCl/AgI composites. Thus it can be suggested that BiOCl/AgI is suitable to excite its electrons under visible light that are required for the catalytic degradation of organic materials.

Furthermore, the band edge locations of BiOCl and AgI were calculated by using the following empirical formula:

$$E_{CB} = X - E_e - 0.5E_g$$

$$E_{VB} = X - E_e + 0.5E_g$$

where E_{CB} and E_{VB} is the valence and conduction band edge potential, X are the electro negativities of BiOCl (X = 6.36) [18] and AgI (X = 5.48) [19]. E_g is the band gap energy of the semiconductor while E_e is the energy of free electrons on the hydrogen scale (about 4.5 eV). The estimated E_{CB} and E_{VB} values were −0.52 and 2.48 for AgI and −0.39 and 3.92 for BiOCl respectively. Therefore, it can be proposed that BiOCl and AgI exhibit a matching interactive energy band structure. These observations support the efficient separation of the charges (electrons and holes) that are originated from AgI in the BiOCl/AgI catalyst [20].

3.5 PL analysis

To investigate the separation and recombination of the charge carriers in the synthesized samples with different BiOCl molar ratios, photoluminescence (PL) was measured (Fig. 5) at room temperature. The BiOCl/AgI composites showed almost similar emission peaks with that of pure AgI. The PL absorbance intensity of AgI and BiOCl around 485 nm was higher in 40BAg sample (Fig. 5). As well known, PL reflects an impressive result to reveal migration, recombination and charge transfer efficiency. There are many reports where the higher PL intensity shows lower recombination of electron hole pairs that reduces the photocatalytic activity. However, sometime a surface defect and oxygen vacancy at the catalyst surface can cause higher PL intensity of photoluminescence and photocatalytic activity [21].

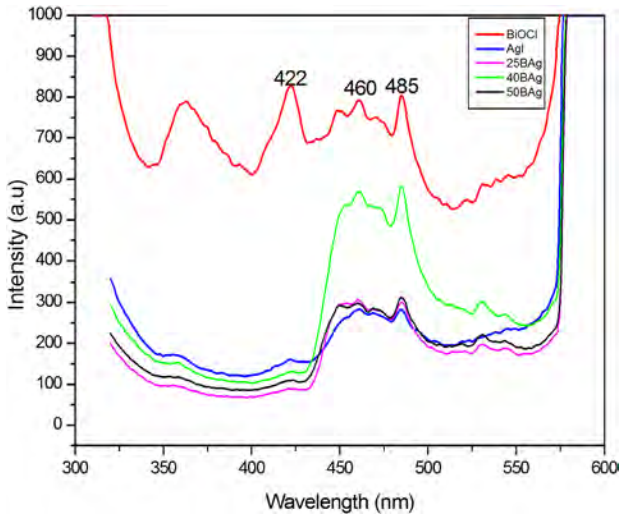

Fig. 5 PL spectra of the synthesized catalysts

3.6 XPS analyses

Figure 6 shows the high resolution XPS spectra of the 40BAg catalyst. The 40BAg sample contains Bi, Cl, O, Ag and I elements (Fig. 6a). An O 1s peak (Fig. 6b) at 527.11 eV belongs to O_2- in the Bi–O bond in BiOCl [21]. Also the broad O 1s peak (Fig. 6c) indicates more than one chemical oxygen species [22]. Two XPS characteristic peaks (Fig. 6d) at 156.87 and 162.13 eV were $Bi4f_{7/2}$ and $4f_{5/2}$ related to Bi^{3+} [23]. The peaks (Fig. 4e) detected at 371.93 and 365.92 eV represents Ag $3d_{3/2}$ and Ag $3d_{5/2}$ of Ag^{+} in the 40BAg sample [24]. The binding energies of 628.65 and 617.24 eV were attributed to $I3d_{3/2}$ and $I3d_{5/2}$ respectively. This confirms the presence of I^{-} in AgI [20] (Fig. 6f). These results confirm the pure BOCl/AgI composite to be used in the photocatalytic study.

3.7 Photocatalytic studies

All photocatalytic studies were performed under UV–Visible irradiation at room temperature and neutral pH. As well known, adsorption of the samples plays a major role in the degradation process. 0.1 g/50 mL of solid/liquid was added to a beaker where the concentration of 3-CP was 10 mgL^{-1}. This solution was kept in the dark for 60 min to obtain adsorption/desorption equilibrium. Initially the absorption spectrum of 3-CP did not change until irradiated by UV–Visible light without catalyst (Fig. 7). The obtained absorption spectra of 3-CP presented a distinct band centered around 269 nm. This band is related to the electronic transitions of the phenolic oxygen on the aromatic ring of 3-CP [25].

In 40BAg sample, similar absorption spectrum of 3-CP was observed in dark conditions. This confirmed that the synthesized samples did not shift the absorption spectra of 3-CP at initial stages. During the photodegradation, a 300 W Xe lamp with cut off UV filter was used as visible light source. For UV light irradiation, a specially designed UV reactor was used that consists of a closed system having a Spectroline XX-15 N UV lamp that emits radiation at 260 nm with the intensity of 2 mW cm^{-2} and allows fixed mixing and cooling. Once photocatalytic degradation had begun, 1 mL of sample was withdrawn and filtered to monitor degradation rates of 3-CP in a spectrophotometer. This process was repeated every 30 min. Photocatalytic degradation of 3-CP was calculated using the following equation:

$$\%\text{Degradation} = \frac{\text{Co} - \text{C}}{\text{Co}} \times 100 = \frac{\text{Ao} - \text{At}}{\text{At}} \times 100$$

where A_o and A_t are the initial and final absorbance of 3-CP at 274 nm for visible light and 269 nm for UV light irradiated samples.

According to the Beer–Lambert law, initial and final absorbance represent the initial (C_o) and final (C) concentrations of 3-CP [26]. The obtained results showed that composite BiOCl/AgI catalyst was more active to degrade 3-CP than the pure BiOCl and AgI samples. The amount of BiOCl was changed up to 50% in the BiOCl/AgI composites (Fig. 7), where 40% of BiOCl content in the composite provided the highest photocatalytic activity. A possible explanation for this might be that more BiOCl content lowers the electron transfer efficiency of the photo-generated electron–hole pairs. So the catalytic activity decreases under the visible light [27]. In addition, more crystalline defect is possible in structure of the 40BAg sample (40%) that is also consistent with data obtained in UV-DRS results. The improved catalytic performance of the catalysts can be connected to several factors such as BET surface area, absorption ability, separation of electron/hole pair oxygen vacancy etc. To explain the photocatalytic mechanism of the BiOCl/AgI samples under UV–Visible irradiation, the band structures of the BiOCl and AgI must be considered.

The visible light degraded 64.1% of 3-CP (10 mgL^{-1}), whereas UV light degraded 71.4% of 3-CP (10 mgL^{-1}) within 120 min for 40BAg sample. The pseudo-first order kinetic rate was used to correlate the experimental results (Fig. 8b, d). The first order kinetic rate k (1/min) for 3-CP degradation can be calculated by plotting $\ln\left(\frac{\text{Co}}{\text{C}}\right)$ versus time (t). $C_0$is the initial concentration at zero time and C stands for the concentration at certain time. The kinetic rate constant and regressions coefficient values are provided in Table 1. Infact, higher rate constant value represents higher degradation yield in a photocatalytic reaction [27]. The obtained rate constant value of 40BAg sample was higher than the other samples (0.0065 and 0.0107 min^{-1} for visible and UV irradiations respectively). These higher kinetic rate

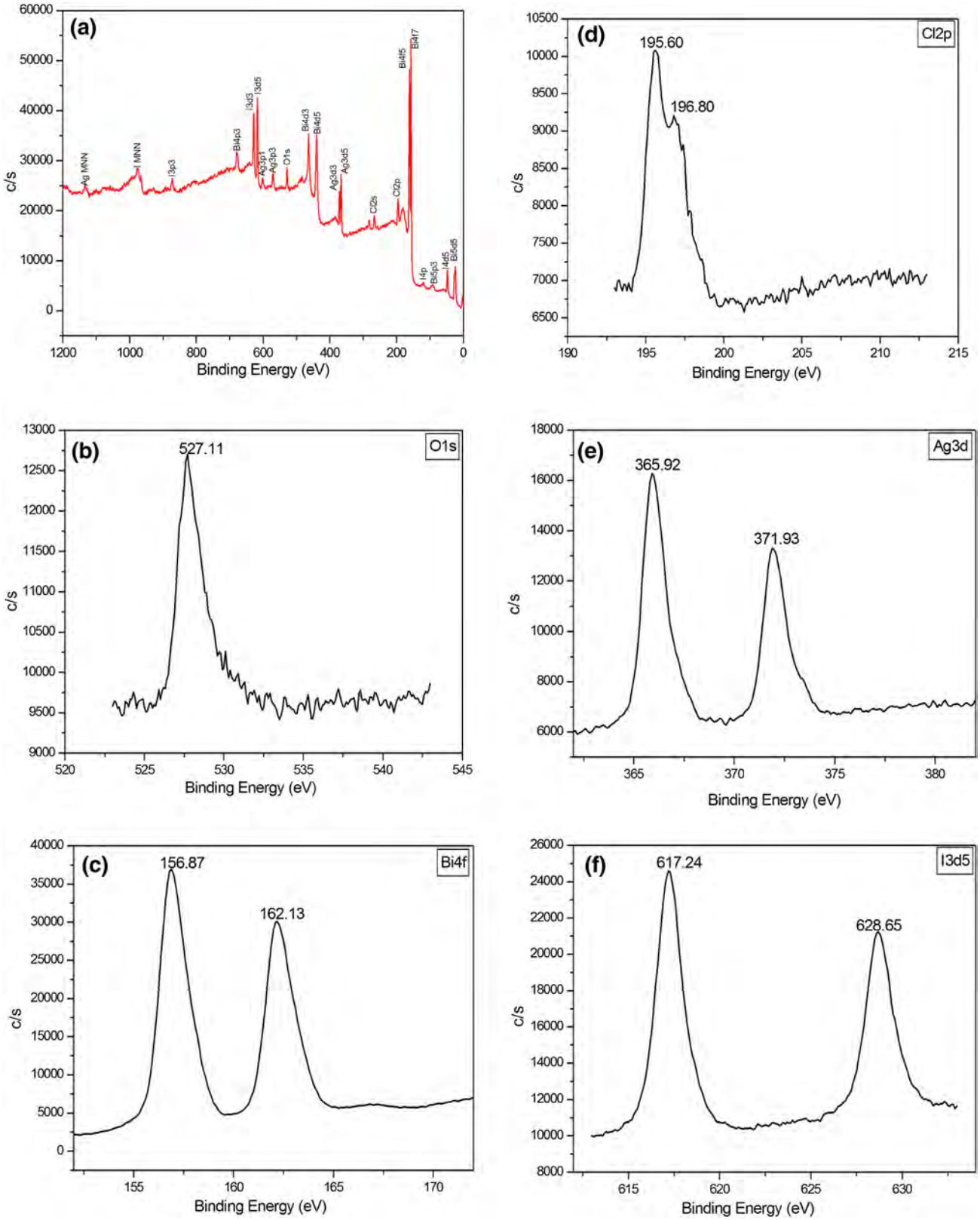

Fig. 6 XPS spectra of 40Bag sample, **a** survey, **b** O1s, **c** Bi4f, **d** Cl2p, **e** Ag3d, **f** I3d

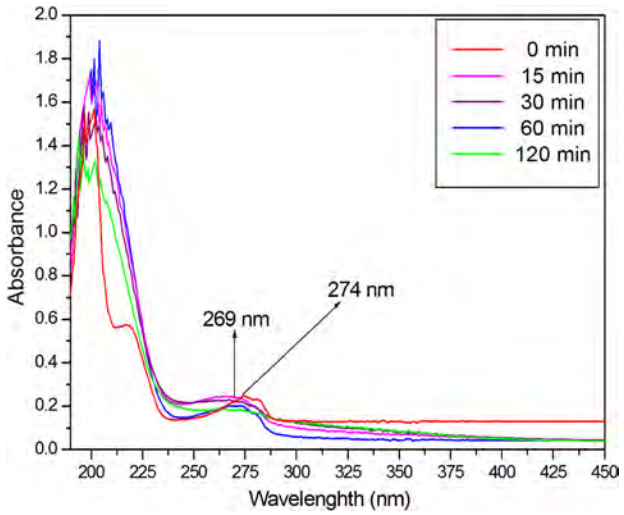

Fig. 7 The absorption spectra of 3-CP under UV light at different degradation time

constants of 40BAg sample show efficient degradation than the others.

The band structure of BiOCl/AgI composites is given in Fig. 9. The obtained VB and CB band edge potential of BiOCl are 3.92 and − 0.39 eV while the VB and CB band potential of the AgI are 2.48 and − 0.52, respectively. Under the visible light irradiation ($\lambda \geq 405$ nm), only the VB electrons of the AgI were excited to its CB level. The excited electrons of AgI transferred to the CB level of BiOCl due to their matching band structure. The standard redox potential of $O_2/\cdot O_2^-$ is approximately − 0.33 [28]. Therefore, transfer of electrons from the CB level of AgI to the BiOCl enables the release of superoxide radicals $\left(\cdot O_2^-\right)$ by reducing $\left(O_2\right)$. Also, the standard redox potential of $H_2O/OH^{\cdot}$ is about 2.38 eV that confirms that the holes (h^+) on the AgI surface oxidizes H_2O to ·OH radical.

The VB electrons of BiOCl are not excited under visible light due to higher band gap, however it plays as an electron trapping center to improve the separation efficiency of electron hole pairs that are originated from AgI catalyst

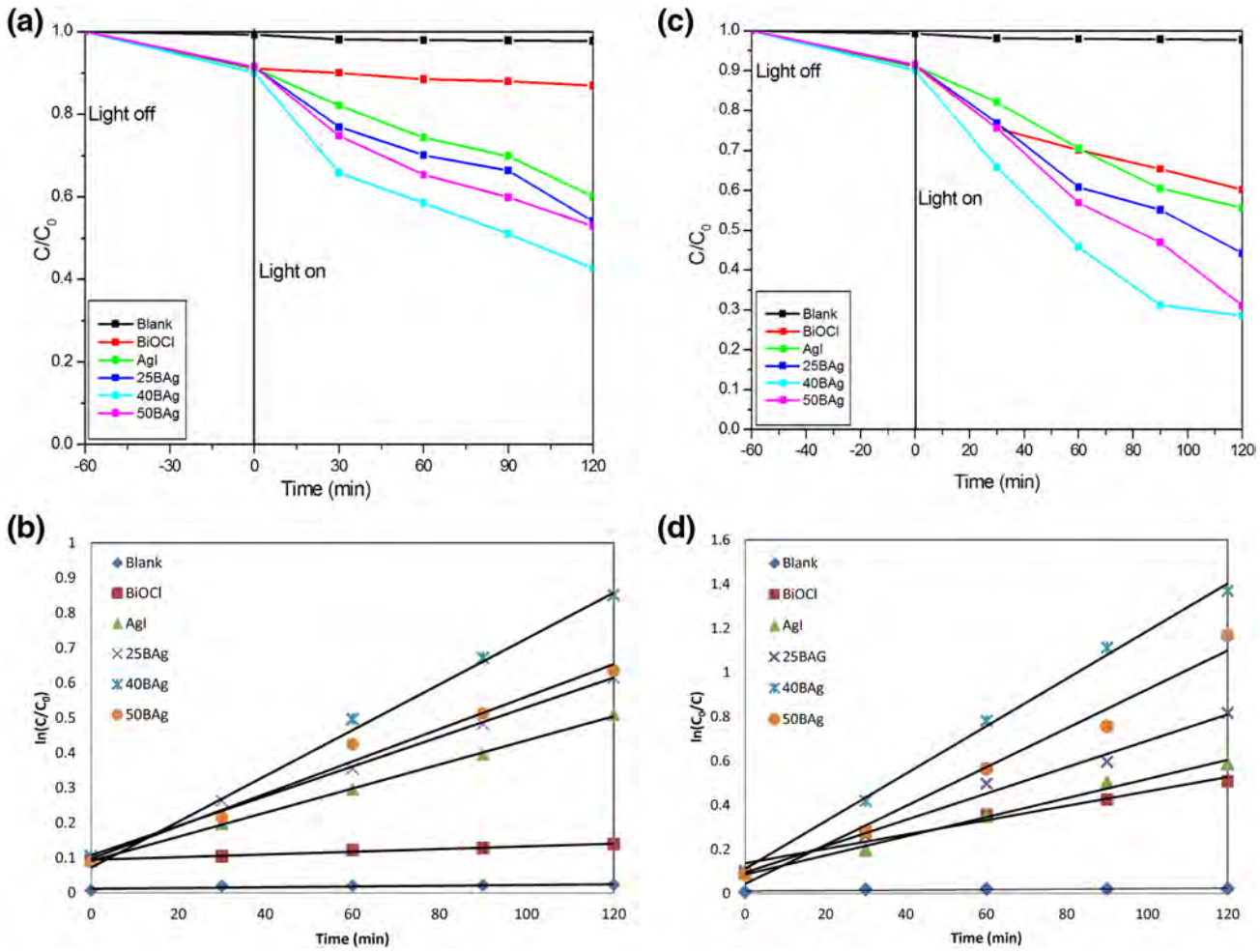

Fig. 8 Photocatalytic degradation of 3-CP and ln (C_0/C) as function of time using the catalysts under visible light (**a, b**), UV light (**c, d**)

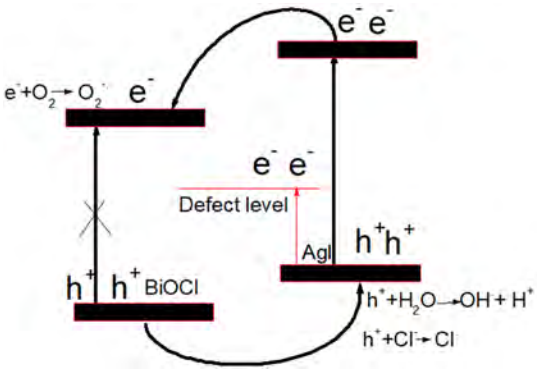

Fig. 9 Schematic illustration of photocatalytic mechanism of 40BAg sample under visible light

(Fig. 9). During this process, AgI particles intercept the photo-induce electrons by interstitial Ag^+ to reveal metallic Ag [20] that improved the catalytic performance of 40BAg catalyst under visible light. Photodegrading of 3-CP under UV irradiation was higher than the visible light. 40BAg similarly exhibited more catalytic activity under both UV and visible irradiation.

From the above discussion, one can understand the following points:

- It is possible that these results are originated from more excited electrons in both VB level of BiOCl / AgI and transferring of the holes in the VB level of BiOCl (Fig. 9).
- When 3-CP adsorbs on the catalyst surface, the electrons in the valence band (VB) of BiOCl and AgI excites to their defect level that lead to PL result. This level exhibits extra hole h^+ in the BiOCl/AgI structure. The oxygen vacancies V_0 can capture a hole $\left(h^+\right)$ in the defect level to transform V_0^+ species [29]. These processes causes efficient separation of electron hole pairs in combination.
- Holes $\left(h^+\right)$ on the BiOCl and AgI can oxidize Cl^- ions to $Cl^{\cdot}$ and I^- ions to $I^{\cdot}$. These radicals can oxidize 3-CP into CO_2 and H_2O. Thus, these coupling radicals shows efficient catalytic activity of the composite BiOCl/AgI samples [23].

Table 2 presents a comparison of photocatalytic degradation yield of AgI based composites. It is clear that AgI based composites exhibited efficient catalytic activity of degradation for some organic pollutant under visible light irradiation. The obtained degradation results can be related to the efficient inhibition of recombination rate of electron/hole pairs and surface plasmon resonance (SPR) of metallic Ag.

3.8 Mechanism of 3-CP degradation over BiOCl/AgI

Radical reactive species (h^+, $O_2^{\cdot-}$ and $OH^{\cdot}$) play an active role to decompose organic pollutants. To evaluate the main reactive species in the 3-CP decomposition, ascorbic acid (AA), potassium iodide (KI) and isopropyl alcohol (IPA) (each 1 mmol L^{-1}) were used as $\left(O_2^{\cdot-}\right)$, (h^+) and $(OH^{\cdot})$ scavengers in the BiOCl/AgI/3-CP system (Fig. 9). The results showed that AA and KI have strongly suppressed the catalytic performance of 40BAg sample under both visible and UV light. These findings suggest that the main reactive species for 3-CP degradation over BiOCl/AgI catalyst are $O_2^{\cdot-}$ and h^+ (Fig. 10).

4 Conclusion

BiOCl/AgI composites were successfully synthesized by in situ precipitation technique. The photocatalytic activity of the composites was evaluated using 3-CP under visible and UV irradiations. BiOCl/AgI composites showed more catalytic activity than pure BiOCl and AgI that can be attributed to the low recombination rate of electron/hole pairs, (Cl^-) and (I^-) ions to produce $(Cl^{\cdot})$ and $(I^{\cdot})$ radicals. BiOCl was found as the electron trapping center under visible light. Photo-generated superoxide radicals and holes were main active species under UV and Visible light. The composites degraded 3-CP with excellent yields. BiOCl/AgI composites are new candidates where the photodegradation of organic pollutants is required. These photocatalysts should be further explored against other water soluble organic pollutants.

Table 2 Comparing photocatalytic degradation yield of AgI based composites

Photocatalyst	Model pollutant	Band gap (eV)	Photocatalytic data (%) Under visible light	Refs.
BiOCl/AgI (40BAg)	3-chloro phenol (3-CP)	E_g (AgI) = 3.01	~65	This study
AgI/BiOI (AgI 4%)	Methyl orange (MO)	E_g (AgI) = 2.34	~70	[28]
p–AgI/{001}*n*–$Bi_2O_2CO_3$	2-chloro phenol (2-CP)	E_g (AgI) = 2.34	~100	[23]
AgI/ZnO (ZnO@AgI-5%)	Methyl orange (MO)	E_g (AgI) = 2.81	~83	[14]

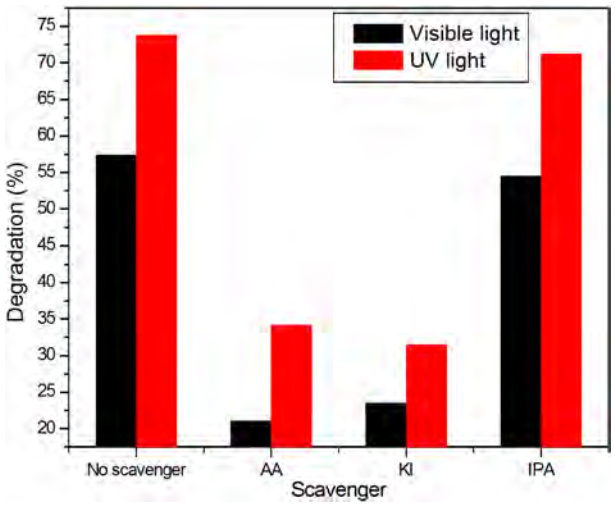

Fig. 10 Effect of scavenger on the 3-CP degradation over BiOCl/ZnO (40BAg)

Acknowledgements This study has been supported by Mugla Sitki Kocman University Coordination of Scientific Research with 15/139.

References

1. L.M.B. Batista, A.J. dos Santos, D.R. da Silva, A.P. de Melo Alves, S. Garcia-Segura, C.A. Martinez-Huitle, Sci. Total Environ. **596**, 79–86 (2017)
2. F. Han, V.S.R. Kambala, M. Srinivasan, D. Rajarathnam, R. Naidu, Appl. Catal. A **359**, 25–40 (2009)
3. G. Zhang, Y. Tan, Z. Sun, S. Zheng, J. Environ. Chem. Eng. **5**(1), 1196–1204 (2017)
4. J. Jiang, H. Wang, X. Chen, S. Li, T. Xie, D. Wang, Y. Lin, J. Colloid. Int. Sci. **494**, 130–138 (2017)
5. B.R. Cruz-Ortiz, J.W. Hamilton, C. Jablos, L. Diaz-Jimenez, D.A. Cortes-Hernandez, P.K. Sharma, M. Castro-Alferez, P. Fernandez-Ibanez, P.S.M. Dunlop, J.A. Byrne, Chem. Eng. J. **316**, 179–186 (2017)
6. H. Kono, R. Kusumoto, J. Water Process. Eng. **7**, 83–93 (2015)
7. J. Yao, D. Wen, J. Shen, J. Wang, J. Water Process. Eng. **11**, 98–103 (2016)
8. A. Fujishima, T.N. Rao, D.A. Tryk, J. Photochem. Photobiol. C **1**(1), 1–21 (2000)
9. Y. Li, Y. Tian, R. Zhang, L. Ma, C. Zhou, X. Tian, Inorg. Chim. Acta. **439**, 123–129 (2016)
10. J. Henle, P. Simon, A. Frenzel, S. Scholz, S. Kaskel, Chem. Mater. **19**(3), 366–373 (2007)
11. A.R. He, S. Cao, P. Zhou, J. Yu, Chin. J. Catal. **35**(7), 989–1007 (2014)
12. S. Fang, C. Ding, Q. Liang, Z. Li, S. Xu, Y. Peng, D. Lu, J. Alloy. Compd. **684**, 230–236 (2016)
13. Z. Song, X. Dong, N. Wang, L. Zhu, Z. Luo, J. Fang, C. Xiong, Chem. Eng. J. **317**, 925–934 (2017)
14. H. Huang, N. Huang, Z. Wang, G. Xia, M. Chen, L. He, C. Ren, J. Colloid Interface Sci. **502**, 77–88 (2017)
15. Z. Xiang, Y. Wang, P. Ju, Y. Long, D. Zhang, J. Alloy Compd. **721**, 622–627 (2017)
16. L. Chen, D. Jiang, T. He, Z. Wu, M. Chen, CrystEngComm **15**(37), 7556–7563 (2013)
17. S. Zhao, Y. Zhang, Y. Zhou, K. Qiu, C. Zhang, J. Fang, X. Sheng, J. Photochem. Photobiol. A **350**, 94–102 (2018)
18. H. Cheng, B. Huang, Y. Dai, Nanoscale **6**(4), 2009–2026 (2014)
19. J. Zhang, Z. Ma, J. Taiwan Inst. Chem. E **81**, 225–231 (2017)
20. H. Ye, H. Lin, J. Cao, S. Chen, Y.J. Chen, Mol. Catal. A **397**, 85–92 (2015)
21. A. Vaizoğullar, Asia-Pac. J. Chem. Eng. **13**, 1–10 (2018)
22. H. Cheng, B. Huang, Y. Dai, Nanoscale **6**, 2009–2026 (2014)
23. L. Zhang, C. Hu, H. Ji, Appl. Catal. B **205**, 34–41 (2017)
24. H. Xu, J. Yan, Y. Xu, Y. Song, H. Li, J. Xia, H. Wan, Appl. Catal. B **129**, 182–193 (2013)
25. N. Salah, A. Hameed, M. Aslam, S.S. Babkair, F.S. Bahabri, J. Environ. Manag. **177**, 53–64 (2016)
26. S. Suwanboon, S. Klubnuan, N. Jantha, P. Amornpitoksuk, P. Bangrak, Mater. Lett. **115**, 275–278 (2014)
27. S. Fang, C. Ding, Q. Liang, Z. Li, Y. Xu Seng, D. Lu, J. Alloy. Compd. **684**, 230–236 (2016)
28. Q. Yang, J. Huang, J. Zhong, J. Chen, J. Li, S. Sun, Curr. Appl. Phys. **171**, 1202–1207 (2017)
29. A. Tabib, W. Bouslama, B. Sieber, A. Addad, H. Elhouichet, M. Férid, R. Boukherrou, Appl. Surf. Sci. **396**, 1528–1538 (2017)